Correlation of chemical coordination and magnetic ordering in $Sr_3YCo_4O_{10.5+\delta}$ (δ=0.02 and 0.26)

D. V. Sheptyakov* and V. Yu. Pomjakushin
Laboratory for Neutron Scattering, ETH Zurich and Paul Scherrer Institut, CH-5232 Villigen PSI, Switzerland

O. A. Drozhzhin, S. Ya. Istomin, and E. V. Antipov
Department of Chemistry, Moscow State University, 119991 Moscow, Russia

I. A. Bobrikov and A. M. Balagurov
Frank Laboratory of Neutron Physics, Joint Institute for Nuclear Research, 141980 Dubna, Russia

(Received 23 January 2009; revised manuscript received 15 April 2009; published 10 July 2009)

The crystal structure and magnetic ordering in $Sr_3YCo_4O_{10.5+\delta}$, δ=0.02 and 0.26 compounds have been revisited in a detailed neutron diffraction study. The ordering is of *G*-type, with the magnetic Co moments being aligned along the *c* axis of the tetragonal cells. In contrast to the previous studies, we, however, find an important peculiarity of the magnetic structures in the title compounds, namely, the magnetic moment magnitudes are different in the layers containing Co ions with different oxygen coordination. Along with the modulation of the coordination type and charge state of Co ions along the *c* axis, the ordered magnetic moment magnitudes are varying concomitantly and thus the correlation between the charge and spin states of the Co ions has been directly observed.

DOI: 10.1103/PhysRevB.80.024409 PACS number(s): 75.25.+z, 61.05.fm, 61.66.Fn

I. INTRODUCTION

The interest to the complex perovskite-related cobalt oxides has been renewed recently in connection with their various interesting physical properties relevant for the potential applications. To mention among them are the metal-insulator transition and the associated large magnetoresistance,[1] and complex magnetic interactions depending on the particular spin state of trivalent or tetravalent cobalt and its coordination in the crystal structure. The type of magnetic interaction may even vary with temperature since for the Co^{3+} ions, a nonmagnetic low-spin ground state with an electronic configuration t_{2g}^6 (S=0) may be thermally excited into the magnetic ones: to the intermediate-spin state with an electronic configuration $t_{2g}^5e_g$ with S=1 or to the high-spin state $t_{2g}^4e_g^2$ with S=2 due to the particularly subtle difference between the intra-atomic exchange energy (Hund's coupling J_H) and the crystal field splitting Δ_{CEF}. The broad magnetic anomalies in $LaCoO_3$ around $T_1 \sim 50$ K and $T_2 \sim 500$ K were interpreted already in the early works by Goodenough as the spin-state transitions.[2–4] Moreover, as it was shown in Ref. 5, the changes in the Co^{3+} spin states affect structural parameters such as the metal-oxygen bond lengths.

Quite recently, the new perovskite-related cobaltites $Sr_{1-x}R_xCoO_{3-y}$, $0.1 \le x \le 0.5$, $0.2 \le y \le 0.4$, R=Y, Sm-Ho, were discovered,[6–9] and an isostructural compound was also reported for the manganite $Sr_{\sim 0.73}Y_{\sim 0.27}Mn_{\sim 0.67}Ga_{\sim 0.33}O_{2.63(1)}$.[10] In the crystal structure of these compounds (possessing tetragonal unit cells with parameters a and c related to the parameter of cubic perovskite a_{per} as $a \approx 2 \times a_{per}$; $c \approx 4 \times a_{per}$), there are three different sites for the A cations occupying two 4*e* positions and one position 8*g*. It was found that Y or rare-earth cations preferentially occupy one of the 4*e* sites. Thus an idealized description of the chemical composition would then be $Sr_3R_1Co_4O_{12-y}$ and this type of structure is now frequently referred to as the 314-phase.[8] Throughout the text we will also call the compounds with the same proportions between the multiplicities of the cation sites just "314 phases".

From the room temperature neutron powder diffraction data it was established[8] that $Sr_{0.7}Dy_{0.3}CoO_{2.62}$ is a *G*-type antiferromagnet with magnetic moments of Co atoms parallel to the *c* axis of the tetragonal structure and the refined magnetic moment value of $1.2\mu_B$ at room temperature for Co atoms. Independently the *G*-type long-range antiferromagnetic (AFM) ordering has been found for $Sr_{0.67}Y_{0.33}CoO_{2.79}$ in Ref. 11. The average for all Co atoms low-temperature value of magnetic moment was found to be equal to $2.0(3)\mu_B$, which corresponds to the intermediate-spin state of Co^{3+}. Based on the magnetization measurements, the authors of Ref. 11 proposed for $Sr_{0.67}Y_{0.33}CoO_{2.79}$ a presence of ferromagnetic regions existing within the long-range-ordered antiferromagnetic matrix as it was originally found for $La_{1-x}Sr_xCoO_3$ in Ref. 12.

Maignan *et al.*[13] measured the electronic properties of cobaltites with close composition of $Sr_{2/3}Y_{1/3}CoO_{8/3-\delta}$. They have established that the heat treatment under oxygen pressure of 100 atm of the as-prepared antiferromagnetic (T_N =290 K) insulator $Sr_{2/3}Y_{1/3}CoO_{2.66}$ led to an increase in the oxygen content up to $O_{2.70}$ and to the transition to ferromagnetic (T_c=225 K) half-metallic state. The ferromagnetic transition in 314 phases was also reported later in Refs. 14–17. In order to reveal the nature of the ferromagnetism in the oxidized 314 phases, A. Baszczuk *et al.*[18] studied the crystal structures of the as-prepared and oxidized $Sr_{2/3}Ho_{1/3}CoO_{3-y}$. Although the oxygen contents in their materials were nearly identical to the ones reported for the ferromagnetic $Sr_{2/3}Y_{1/3}CoO_{8/3-\delta}$ in Ref. 13, no ferromagnetic ordering has been observed.

Here we present a detailed neutron diffraction study of atomic and magnetic structures of the Y-314 phases $Sr_3YCo_4O_{10.5+\delta}$ (or $Sr_{0.75}Y_{0.25}CoO_{2.625+\delta/4}$) with two different oxygen contents: close to ideal ("as-prepared" sample, δ =0.02) and a higher one ("oxidized" sample, δ=0.26). For

both compounds the *G*-type AFM state was confirmed with different long-range magnetic moments for different Co sites and without any indications for the long-range ferromagnetic order with substantial moment magnitudes.

II. SYNTHESIS AND EXPERIMENTAL TECHNIQUES

The $Sr_3YCo_4O_{10.5+\delta}$ sample (as-prepared sample, about 6 g) was synthesized from the intimately mixed stoichiometric amounts of $SrCO_3$, Co_3O_4, and Y_2O_3 pressed into pellets and heated at 1150 °C for 24 h, then reground and reheated at 1170 °C for 48 h. In order to prepare the 314 phase with higher oxygen content, the as-prepared sample (about 3 g) was placed in alumina crucible and heated at 600 °C for 12 h under oxygen pressure of 150 atm.

Initial phase analysis of the samples was performed by x-ray powder diffraction. The patterns were recorded with an imaging plate Huber G670 Guinier camera with Cu K_{α_1} radiation. The oxygen content of the as-prepared and oxidized $Sr_3YCo_4O_{10.5+\delta}$ samples was determined by iodometric titration. About 50 mg of the sample was placed in a flask containing 20 ml of a 20% water solution of KI. Then, several drops of concentrated HCl were added to the solution. The flask was kept in a dark place until the entire sample had dissolved. The released elementary iodine was titrated by a standard $Na_2S_2O_3$ solution with starch added as an indicator. The oxygen content of the samples determined by this procedure corresponds to the formula $Sr_3YCo_4O_{10.5+\delta}$, with $\delta \approx 0.02$ and 0.26 for the as-prepared and oxidized samples, correspondingly.

The synchrotron x-ray diffraction measurements were carried out at the Materials Sciences beamline of the Swiss Light Source with the wavelength $\lambda = 0.8$ Å at room temperature and did allow for sorting out the small amounts of impurities. According to the results of the Rietveld refinements carried out on the synchrotron x-ray data, both samples contained admixtures of CoO (~1% weight) and Y_2O_3 (the as-prepared sample ~0.3% weight and the oxidized one—~0.5% weight).

The ac magnetic susceptibility and the magnetization in permanent external magnetic fields were measured using the Quantum Design PPMS apparatus. The ac susceptibility was measured in zero external magnetic field with the amplitude of the exciting ac field of 10 Oe at 1 kHz frequency. The ac susceptibility curves are shown in Fig. 1. The measurements were carried out on heating the samples between 2 and 400 K. The as-prepared sample shows an antiferromagnetic transition at ~335 K, together with another broad maximum at ~275 K, of a still unknown nature. The oxidized sample shows the (AFM) transition 290 K. Thus, the Néel temperature decreases by ~45 K upon oxidation of the 314 phase. The absolute amplitude of the signal close to the transition is about twice lower for the oxidized sample, compared to the as-prepared one. It should be noted that the values of the ac susceptibility for both samples are in fact very low—between 0.04 and 0.08 emu/mole.

Antiferromagnetic type of ordering in the as-prepared and oxidized samples of $Sr_3YCo_4O_{10.5+\delta}$ is supported by the measured dependences of the bulk magnetization in permanent external magnetic fields at several selected temperatures. For illustration, in Fig. 2, we present them for the as-prepared sample. At room temperature (just below but close to the AFM transition point of the as-prepared $Sr_3YCo_4O_{10.52}$ sample), the field-increasing and field-decreasing dependences of the bulk magnetization are not ideally coinciding, while in the ordered magnetic state ($T = 8$ K) they are practically indistinguishable. It is important to note here that we were sampling the magnetic field on purpose with a logarithmic scale (i.e., choosing the steps in magnetic field such that $\log_{10}|H|$ were constant, thus sampling the low-fields limit with high precision) in order to be able to notice the possible hysteresis loops at low fields. These were however not detected in either of the cases—at least down to the precision of the magnetic field settling (~0.2 Oe). The same result—absence of hysteresis loops at different temperatures—was also obtained for the oxidized sample. Thus, we can exclude the possibility of the bulk ferromagnetism in the investigated phases.

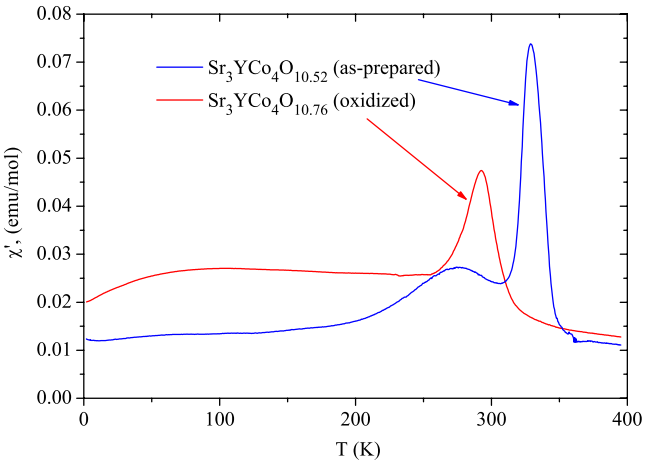

FIG. 1. (Color online) The ac magnetic susceptibility data for the as-prepared and oxidized samples of $Sr_3YCo_4O_{10.5+\delta}$.

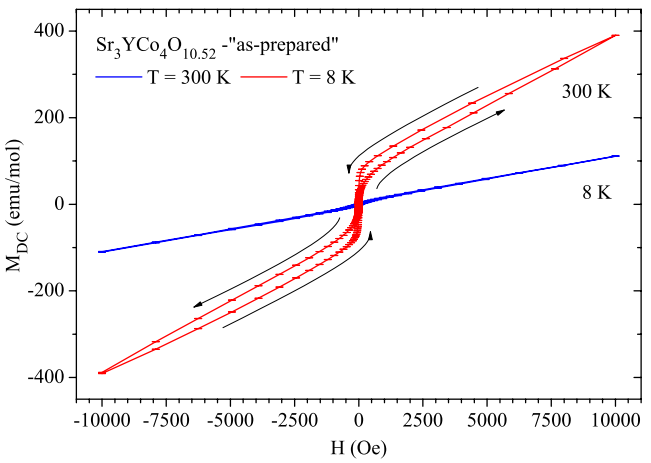

FIG. 2. (Color online) Magnetic field dependences of the bulk magnetization in permanent magnetic fields measured at $T = 300$ K and $T = 8$ K for the $Sr_3YCo_4O_{10.52}$ (as-prepared sample). The arrows indicate the direction of the field changes for the only case where the magnetization and demagnetization curves are obviously not coinciding.

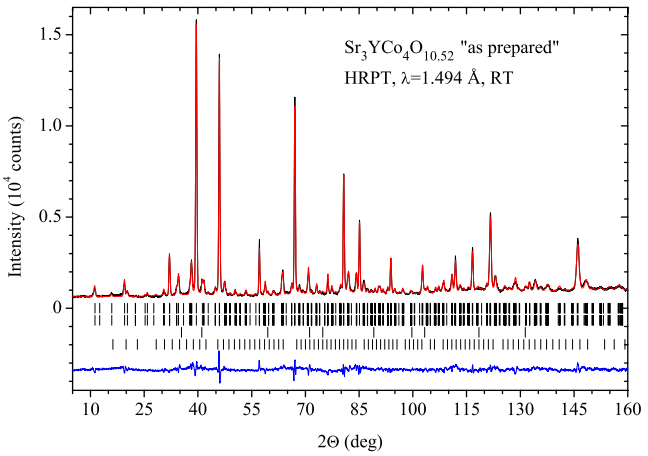

FIG. 3. (Color online) A representative Rietveld refinement plot from the HRPT neutron powder diffraction data of $Sr_3YCo_4O_{10.52}$ (as-prepared sample) measured with $\lambda=1.494$ Å at room temperature. The experimental data, the calculated profile and the difference curve are shown. The four rows of ticks indicate the calculated peak positions for (from top to bottom): the crystalline phase, the magnetic phase contribution, the CoO, and Y_2O_3 impurities.

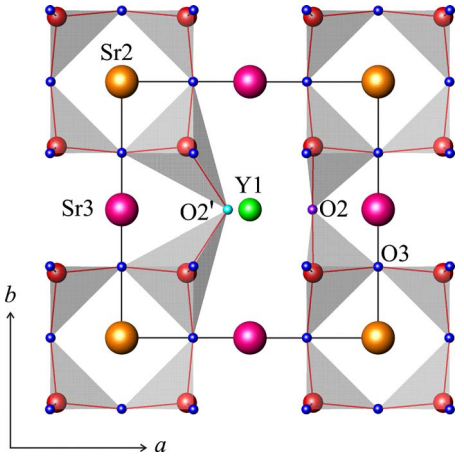

FIG. 4. (Color online) One of the possible arrangements of oxygen atoms in oxygen-deficient layer ($z=1/2$) in the 314 phases.

Neutron diffraction patterns were collected with the powder diffractometers HRPT (Ref. 19) and DMC (Ref. 20) both located at SINQ spallation neutron source, PSI Villigen, in wide temperature ranges. HRPT is a high-resolution neutron diffractometer with the ultimate instrument resolution $\Delta d/d$ of about 0.001, which promotes precise analysis of the crystal structure parameters and peak broadening effects. Neutron powder diffraction with cold neutrons ($\lambda=2.45$ Å) at DMC diffractometer was used for determining the low-temperature magnetic structure. Crystal structure refinement with thermal neutrons at HRPT diffractometer was performed with three different wavelengths ($\lambda=1.155$, 1.494, and 1.886 Å) at room temperature for both samples. Additionally, the temperature scan of the crystal structure parameters with the high-intensity mode of HRPT ($\lambda=1.494$ Å) has been carried out for the oxidized sample. For the as-prepared sample, an additional temperature scan with cold neutrons ($\lambda=2.955$ Å) was performed at HRPT in order to complete the temperature dependence of the magnetic structure measured with DMC diffractometer. The refinements of the crystal and magnetic structure parameters were carried out with FULLPROF program suite,[21] with the use of its internal tables for scattering lengths and magnetic form factors. An example of the typical diffraction pattern measured at HRPT and treated with Rietveld method is given in the Fig. 3.

III. RESULTS AND DISCUSSION

The laboratory and synchrotron x-ray, as well as the neutron diffraction patterns of both samples at all temperatures, were indexed in a tetragonal unit cell with the $I4/mmm$ (No. 139) space group. The unit-cell parameters at room temperature are close for the as-prepared and oxidized samples: $a=7.6508(3)$, $c=15.3205(6)$ Å, and $a=7.6431(3)$, $c=15.3151(2)$ Å, respectively. The relation $c\approx 2\times a$ is fulfilled with high precision for both samples.

A. Neutron diffraction results: Crystal structure of $Sr_3YCo_4O_{10.5+\delta}$ at room temperature

The crystal structures of $Sr_3YCo_4O_{10.5+\delta}$ (as-prepared and oxidized samples) were refined at 298 K using neutron diffraction data from HRPT diffractometer and the structural model from Ref. 7. In our refinements, we considered the difference in neutron scattering lengths of Sr ($b_{Sr}=7.02$ *fm*) and Y ($b_Y=7.75$ *fm*) to be too tiny in order to refine their possible mutual substitutions. Hence, we have positioned the smaller Y^{3+} cations exclusively in the *A* positions $4e(0,0,\sim 0.14)$ with the lowest effective coordination number. The two other *A* positions are occupied in our refinement model exclusively by the Sr^{2+} cations: $4e(0,0,\sim 0.62)$ and $8g(0,0.5,\sim 0.13)$.

As it was revealed earlier, there are two positions where oxygen atoms in the oxygen-deficient layer of the crystal structure of 314 phases could be located (Fig. 4).[18,22] In an ideal perovskite, the position for oxygen atoms would be $(\sim 0.25,0,0)$ or, equivalently, $(\sim 0.75,0.5,0.5)$ as for the O2 shown in Fig. 4. In Refs. 6, 8, 10, and 18 it was found that in the crystal structure of 314 phases oxygen atoms are shifted from position O2 to $(\sim 0.1,0,0)$ position, as for the O2′ which is shown in Fig. 4 in the equivalent site $(\sim 0.4,0.5,0.5)$. This happens because of the necessity to shorten interatomic distances between oxygen and small *A*-site cation such as Y^{3+} positioned at $4e(0,0,\sim 0.14)$ [shown in Fig. 4 in an equivalent position $(0.5,0.5,\sim 0.64)$].

At the initial stage of the refinement of the crystal structure of the as-prepared phase, we have considered that oxygen atoms occupy position O2′, as in the crystal structure of $Sr_{0.7}Y_{0.3}CoO_{2.62}$.[6] However, refinement of the atomic coordinate of O2′ with fixed occupancy and atomic displacement parameter (ADP), led to the value $(\sim 0.19,0,0)$. Attempts to refine the occupancy and ADP of this oxygen atom resulted in the physically unreasonable values. Therefore we have assumed that oxygen atoms in the oxygen-deficient layer are distributed over both the O2 and O2′ positions. A strong

TABLE I. Crystal and refinement data for $Sr_3YCo_4O_{10.52}$ (as prepared) and $Sr_3YCo_4O_{10.76}$ (oxidized) at 298 K. For each of the two samples, the results are obtained from the combined refinement of three datasets collected in the angular range 5…165° with different neutron wavelengths: λ=1.155, 1.494, 1.886 Å. Space group is $I4/mmm$ (Z=4).

Sample	As prepared	Oxidized
Lattice parameters:		
a, Å	7.6508 (3)	7.6431 (3)
c, Å	15.3205 (6)	15.3151 (6)
V,Å^3	896.78 (6)	894.66 (6)
R_p,R_{wp},χ^2 (λ=1.155 Å)	4.39%, 5.63%, 3.20	4.23%, 5.42%, 3.51
R_p,R_{wp},χ^2 (λ=1.494 Å)	5.37%, 6.85%, 5.55	4.91%, 6.32%, 5.80
R_p,R_{wp},χ^2 (λ=1.886 Å)	5.70%, 7.52%, 7.29	5.34%, 6.94%, 6.10
Global χ^2 (Bragg contrib.)	5.40	5.19

correlation between the positional parameters and occupancies of these closely located [d(O2−O2′)∼1.1 Å] oxygen atoms was observed during the refinements. Therefore, it was decided to constrain the total occupation of these two positions in such a way that the total oxygen content would match to the results of the iodometry, while the partial occupations of the O2 and O2′ positions had been left to refine.

Crystal and refinement data for both samples are given in Table I. The refined atomic parameters and the main interatomic distances at room temperature are listed in Tables II and III, correspondingly.

There is an important difference in the distribution of oxygen atoms in the oxygen-deficient layers of the presently investigated $Sr_3YCo_4O_{10.52}$ and of the previously reported 314 phases with close oxygen stoichiometry. In Table IV we have summarized atomic coordinates and occupancies of the positions of oxygen atoms O2 and O2′ (Fig. 4) in the different 314 phases, whose crystal structures were refined using neutron powder diffraction data. In the case of the 314 phases with oxygen stoichiometry close to $O_{10.5}$ ($O_{2.625}$ in notations of $Sr_{1-x}R_xCoO_{3-y}$), only the position O2′ is occupied and its occupancy corresponds within the $e.s.d.$ to the ideal value: 0.25. Additional to the $O_{10.5}$ oxygen atoms are distributed over the O2 positions, whose occupancy increases with oxygen content. In the case of the as-prepared $Sr_3YCo_4O_{10.52}$ the situation is different. In spite of the close to $O_{10.5}$ oxygen stoichiometry of the phase, oxygen atoms are distributed with nearly equal probabilities over the O2 and O2′ positions (see Table II). Shifting of the oxygen atoms from position O2′ to O2 (Fig. 4) means substantial elongation of the interatomic bonds between cations in Y1 position and oxygen atoms in the layer [d(Y1−O2)=2.863(5), d(Y1−O2′)=2.296(11) Å]. Therefore, one can suppose that the main reason for the presence of oxygen atoms in O2 position is a considerable amount of larger Sr^{2+} cations in the Y1 position. This high degree of disorder in the distribution of Sr and Y in the structure of $Sr_3YCo_4O_{10.52}$ could be due to the higher temperature used for the preparation of the compound together with higher Sr/Y ratio than for $Sr_{0.7}Y_{0.3}CoO_{2.62}$.[6] The assumption that the amount of oxygen in O2′ position could be determined by the amount of Y^{3+} in Y1 position is supported by the fact that, upon oxidation of the $Sr_3YCo_4O_{10.52}$, i.e., in the oxidized sample $Sr_3YCo_4O_{10.76}$, oxygen atoms are introduced into the O2 position, while occupancy of the O2′ remains within

TABLE II. Atomic coordinates, displacement parameters (Å^2), and site occupancies for the $Sr_3YCo_4O_{10.52}$ (as prepared) and $Sr_3YCo_4O_{10.76}$ (oxidized) at 298 K. The fractional occupancies of all atoms apart from O2 and O2′ are equal to unity.

Atom, site		As prepared	Oxidized
Y1 $4e(0,0,z)$	z	0.1430 (4)	0.1422 (4)
	B, Å^2	1.59 (12)	1.62 (12)
Sr2, $4e(0,0,z)$	z	0.6204 (6)	0.6208 (5)
	B, Å^2	1.71 (13)	1.55 (12)
Sr3, $8g(0,\frac{1}{2},z)$	z	0.1324 (3)	0.1318 (3)
	B, Å^2	0.77 (7)	0.71 (6)
Co1, $8h(x,x,0)$	x	0.2461 (8)	0.2463 (8)
	B, Å^2	0.85 (17)	0.71 (15)
Co2, $8f(\frac{1}{4},\frac{1}{4},\frac{1}{4})$	B, Å^2	0.55 (15)	0.57 (14)
O1, $16m(x,x,z)$	x	0.2194 (4)	0.2204 (4)
	z	0.1168 (3)	0.1180 (3)
	B, Å^2	3.11 (11)	3.10 (9)
O2, $8i(x,0,0)$	x	0.241 (5)	0.244 (3)
	B, Å^2 [a]	1.05 (5)	1.08 (4)
	Frac. occ.	0.136 (8)	0.232 (8)
O2′, $8i(x,0,0)$	x	0.090 (4)	0.087 (3)
	B, Å^2 [a]	1.05 (5)	1.08 (4)
	Frac. occ.	0.124 (8)	0.148 (8)
O3, $8j(x,\frac{1}{2},0)$	x	0.2226 (7)	0.2222 (7)
	B, Å^2 [a]	1.05 (5)	1.08 (4)
O4, $16n(0,y,z)$	y	0.2476 (4)	0.2478 (4)
	z	0.2584 (3)	0.2576 (3)
	B, Å^2 [a]	1.05 (5)	1.08 (4)

[a]Atomic displacement parameters for the atoms O2, O2′, O3, and O4 (atoms in the CoO_2 and $CoO_{\sim 1.25}$ planes perpendicular to the c axis) were constrained to equality in the refinements.

TABLE III. Selected interatomic distances (Å) in $Sr_3YCo_4O_{10.52}$ (as prepared) and $Sr_3YCo_4O_{10.76}$ (oxidized) at 298 K.

Bond	As prepared	Oxidized
Y1-O1	2.408(3)×4	2.411(3)×4
Y1-O2[a]	2.863(5)×4	2.867(5)×4
Y1−O2′ [a]	2.296(11)×4	2.277(5)×4
Y1-O4	2.591(6)×4	2.590(6)×4
Sr2-O1	3.037(3)×4	3.023(3)×4
Sr2-O3	2.812(7)×4	2.816(6)×4
Sr2-O4	2.653(8)×4	2.656(7)×4
Sr3-O1	2.736(3)×4	2.729(3)×4
Sr3-O2[a]	2.836(3)×2	2.811(3)×2
Sr3-O3	2.649(5)×2	2.638(5)×2
Sr3-O4	2.730(5)×2	2.725(5)×2
Sr3-O4	2.555(4)×2	2.566(4)×2
Co1-O1	1.813(5)×2	1.827(5)×2
Co1-O2[a]	1.883(6)×2	1.883(6)×2
Co1−O2′ [a]	2.230(17)×2	2.242(14)×2
Co1-O3	1.951(8)×2	1.948(8)×2
Co2-O1	2.067(5)×2	2.048(5)×2
Co2-O4	1.917(3)×4	1.914(3)×4

[a]Partially occupied oxygen positions (details in Table II).

$2\times e.s.d.$ the same as in the as-prepared one (Table II). We can therefore assume that the degree of ordering of large and small *A*-site cations in 314 phases could be tuned by different preparation routes and this may influence the local coordination environment of cobalt in the oxygen-deficient layers and the physical properties of the material. The later statement is supported by the paper of Fukushima *et al.*[23] published during the preparation of the present manuscript, where different magnetic and transport properties of the *A*-site ordered and disordered Y-314 phases were reported.

B. Temperature evolution of the crystal structures of $Sr_3YCo_4O_{10.52}$ and $Sr_3YCo_4O_{10.76}$

The temperature dependences of the unit cell parameters for the investigated samples are presented in the Fig. 5. It should be noted that while at low temperatures the thermal expansion of the lattice in all samples is approximately isotropic, it becomes strongly anisotropic with $\alpha_c \gg \alpha_a$ at higher temperatures. Similar anisotropic behavior of the thermal expansion of the crystal structures of the Y-314 phases has also been observed at higher temperatures up to 900 °C.[24]

This high anisotropy of the thermal expansion of the 314 structure could be due to the changes in the tilting angles of the cobalt-oxygen polyhedra with temperature. However, the analysis of the temperature dependences (here we refer to the results obtained for the oxidized sample $Sr_3YCo_4O_{10.76}$) of the Co2–O4–Co2 and Co1–O3–Co1 bond angles (between the "completely filled" $Co2O_6$ octahedra and between the "incomplete" $Co1O_{\sim 4.5}$ polyhedra in the in-plane directions) shows that they remain nearly unchanged with temperature. The same is actually true also for the bond angles in the "apical" direction: both the Co1–O1–Co2 angle between $Co2O_6$ octahedron and $Co1O_{\sim 4.5}$ polyhedron and the O1–Co1–O1 angle inside the $Co1O_{\sim 4.5}$ polyhedron stay equal to ~162° in the whole temperature range (value for the oxidized 314 phase).

TABLE IV. Coordinates and occupancies of the oxygen positions O2 and O2′ [$8i(x,0,0)$] in the crystal structure of different compounds which can be classified as 314 phases refined from neutron powder diffraction data. Where necessary, the simple calculations have been carried out in order to match the setting and numbering of the atoms to the one in our table, e.g., the atoms listed as O2′ and O2 were named O3 and O3′ correspondingly in Ref. 18.

Composition	Oxygen position	*x* coordinate	Occupancy	Ref.
$Sr_{0.7}Y_{0.3}CoO_{2.62}$	O2′	0.101(3)	0.23(1)	6
$Sr_{0.7}Dy_{0.3}CoO_{2.62}$	O2′	0.113(4)	0.23(1)	8
$Sr_{\sim 0.73}Y_{\sim 0.27}Mn_{\sim 0.67}Ga_{\sim 0.33}O_{2.63(1)}$	O2′	0.104(1)	0.26(1)	10
$Sr_{0.75}Y_{0.25}Co_{0.75}Ga_{0.25}O_{2.63(1)}$	O2′	0.111(1)	0.25(1)	22
$Sr_{0.67}Ho_{0.33}CoO_{2.67}$	O2′	0.1053(25)	0.295(14)	18
	O2	0.2835(143)	0.063(13)	
$Sr_{0.67}Ho_{0.33}CoO_{2.71}$	O2′	0.10934(229)	0.268(13)	18
	O2	0.29615(557)	0.142(13)	
$Sr_{0.67}Ho_{0.33}CoO_{2.80}$	O2′	0.1487(26)	0.285(11)	18
	O2	0.2916(25)	0.315(12)	
$Sr_{0.75}Y_{0.25}Co_{0.5}Fe_{0.5}O_{2.69(2)}$	O2′	0.100(2)	0.249(8)	22
	O2	0.263(4)	0.151(8)	
$Sr_3YCo_4O_{10.52}$ (as prepared)	O2′	0.090(4)	0.124(8)	Present study
	O2	0.241(5)	0.136(8)	
$Sr_3YCo_4O_{10.76}$ (oxidized)	O2′	0.087(3)	0.148(8)	Present study
	O2	0.244(3)	0.232(8)	

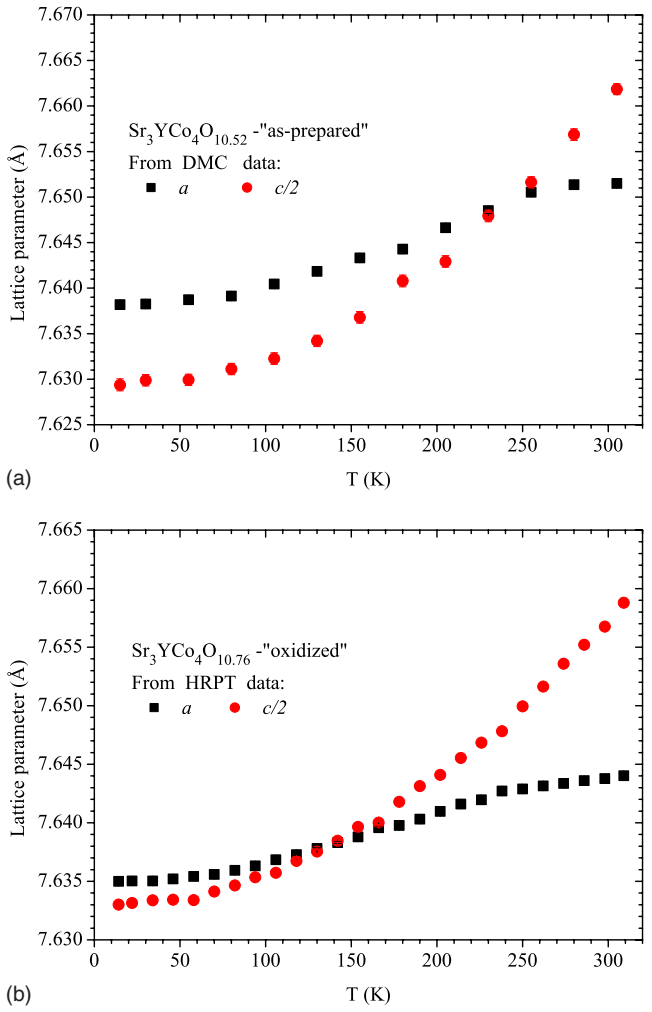

FIG. 5. (Color online) Temperature dependences of the lattice parameters a (squares) and $c/2$ (circles) for the investigated samples: $Sr_3YCo_4O_{10.52}$ (as prepared—panel a), $Sr_3YCo_4O_{10.76}$ (oxidized—panel b).

The main contribution to this anisotropic thermal expansion is in fact the anisotropy of the Co–O bonds expansion in the $Co2(O1,O4)_6$ octahedron (see Fig. 6 for details). We found that the only bond distance which is temperature dependent is the one between cobalt and apical oxygen atoms (Co2–O1) in the completely filled octahedra $Co2(O1,O4)_6$. It increases from ~2.035(5) Å at 14 K to ~2.050(5) Å at 298 K, while in the equatorial direction the Co2–O4 bond distances remain nearly constant: 1.913(3) and 1.914(3) Å at 14 and 298 K, correspondingly. Both the apical and the equatorial bond distances in the Co1 coordination polyhedron remain also the same temperature insensitive.

C. Magnetic structure of $Sr_3YCo_4O_{10.5+\delta}$

Upon cooling, the magnetic peaks appear in the neutron diffraction patterns of both samples in a similar manner. This is illustrated for the oxidized compound in Fig. 7. The positions of all magnetic Bragg peaks marked by numbers in Fig. 7 coincide with those of the nuclear ones: 1—with (110), 2—with (112), 3—with (312)/(116), and 4—with (332)/

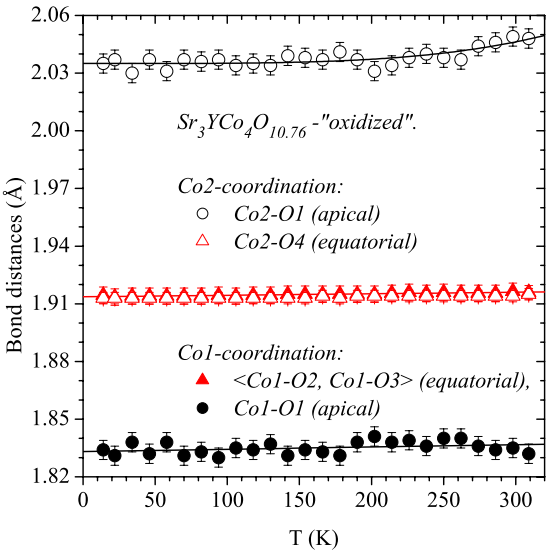

FIG. 6. (Color online) The temperature dependences of the bond distances around Co1 (filled symbols) and Co2 (open symbols) atoms in the $Sr_3YCo_4O_{10.76}$ oxidized compound. The lines are guides for eye. Note that the apical Co1-O1 bond is shorter than the equatorial ones for the Co1 ions in the incompletely filled polyhedra, while in the completely filled octahedra, the apical Co2–O1 bond is much longer than the equatorial Co2–O4 one. The equatorial bond lengths for both Co1 and Co2 atoms are very close to each other (the opened and filled triangles are hardly distinguishable on the graph).

(316). The peak marked with * corresponds to the $(\frac{1}{2},\frac{1}{2},\frac{1}{2})$ magnetic diffraction peak of the CoO impurity and is not within the metrics of the Y-314 compound.

Since the positions of magnetic peaks coincide with those for the allowed nuclear reflections, we conclude that the propagation vector of the magnetic structure of 314-phase is $\kappa=[0,0,0]$. Using the determined propagation vector, we have performed the symmetry analysis of the possible magnetic ordering schemes which has been carried out with the

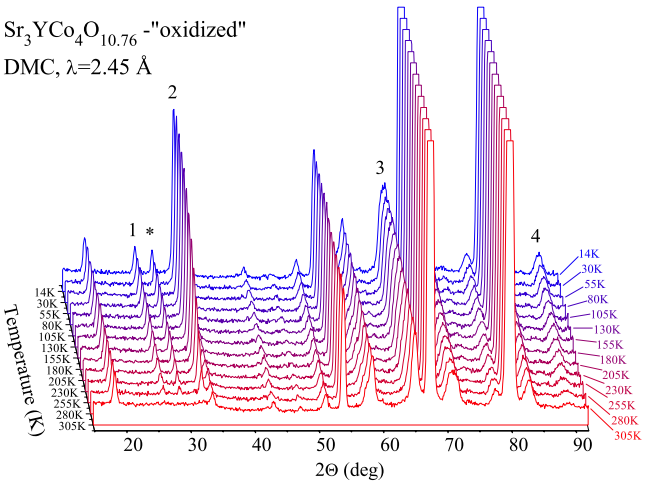

FIG. 7. (Color online) The evolution of the neutron diffraction patterns (taken with DMC powder neutron diffractometer, $\lambda=2.45$ Å) of the oxidized $Sr_3YCo_4O_{10.76}$ compound with temperature. The magnetic peaks are marked with numbers 1–4.

program SARA*h*–2K.[25] An important assumption done was that for both magnetic Co sites, the ordering occurs with one and the same irreducible representation (IR). This leaves out exactly three IRs, for which the decomposition for both Co sites has nonzero coefficients. The basis vectors of the IRs entering the decompositions for both sites with nonzero coefficients simultaneously are given in Table V. From the analysis it follows that (in notations of SARA*h*), the magnetic transition should involve one of the following three irreducible representations: Γ_3, Γ_5, or Γ_9.

The best fit (Fig. 8) to the observed intensities in the neutron powder diffraction patterns was obtained for the magnetic ordering scheme in which the magnetic moments of Co1 are aligned along *c*, Co2 moments may have both the *c* and $a-b$ components (the Γ_5 representation). The symmetry-allowed in-plane (along the $a-b$ diagonals) components of the Co2 magnetic moments are refined to the diminishingly small values and thus have been excluded from the refinements. It should be noted that we cannot completely rule out the possibility for these components in reality to have finite values, but they in any case are very small, if any. An important finding is that the magnetic moments on the two sites are really different. The refined *c*-components of magnetic moments of the two sorts of atoms (Co1 and Co2) are in roughly the 2:1 proportion. The presence of a peak (110) at $2\Theta \sim 26.3°$ (marked as "1" in Fig. 7) unambiguously proves that the Co ions in different sites (Co1 and Co2) are in fact carrying different magnetic moments (its calculated intensity would have dropped to the exact zero if the moments on two Co sites were assumed equal). A hypothetical assumption of the equal magnetic Co moment magnitudes on the two Co sites really seriously poisons the refinements. For example, for the refinement represented in the Fig. 8 (data on the oxidized sample taken with DMC diffractometer at $T=14$ K), the χ^2 value would have raised from 5.36 to 6.95, the profile *R*-factor R_p would have grown from 3.94 to 4.18, and the weighted profile *R*-factor R_{wp}—from 5.25 to 5.98, if one would assume equal moment magnitudes for the two Co sites. We note here that in the earlier papers (Refs. 8 and 11), this very feature of nonequal moment magnitudes for the two Co sites has been overlooked. In fact, in Fig. 5 of Ref. 11, the (110) peak is obviously absent at 350 K and definitely present at 10 K, but it is not modeled by the proposed in Ref. 11 magnetic structure model with magnetic moments equal for all Co ions, and is certainly visible in the difference curve for the 10 K refinement. We have to admit that from our powder diffraction data it is not possible to deduce which exactly of the two atoms—Co1 or Co2 possesses the larger magnetic moment magnitude since both possibilities provide roughly the same refinement quality. However since the Co1 atoms in the oxygen-deficient layers have a lower coordination number (on average 4.5) and thus are "less oxidized", one can assume higher magnetic moments for them in comparison to the Co2 atoms in the octahedral coordination. The magnetic ordering in both samples occurs in the same manner so all the considerations given above are also valid for the as-prepared sample as well. The illustration of the magnetic ordering scheme is given in Fig. 9, along with the drawing of the unit cell of the crystal structure.

TABLE V. Basis vectors (BV) of the irreducible representations (IRs) $\Gamma_3^1, \Gamma_5^1, \Gamma_9^2$ of the little group of propagation vector $\kappa=[0,0,0]$ for the space group $I4/mmm$. Assuming only those IRs relevant which enter with nonzeroed coefficients into the decompositions for both atoms—Co1 and Co2 simultaneously, the decomposition of the axial-vector representations for the 8*h* site (Co1) reads as $\Gamma_{Mag}=1\Gamma_3^1+1\Gamma_5^1+2\Gamma_9^2$, and for the 8*f* site (Co2)—as $\Gamma_{Mag}=2\Gamma_3^1+2\Gamma_5^1+3\Gamma_9^2$. The atoms of the nonprimitive basis are defined as follows. For the Co1 site: 1: $(\sim 0.247, \sim 0.247, 0)$, 2: $(\sim 0.247, \sim 0.753, 0)$, 3: $(\sim 0.753, \sim 0.247, 0)$, and 4: $(\sim 0.753, \sim 0.753, 0)$, and for the Co2 site: 5: $(\frac{1}{4}, \frac{1}{4}, \frac{1}{4})$, 6: $(\frac{1}{4}, \frac{3}{4}, \frac{3}{4})$, 7: $(\frac{3}{4}, \frac{1}{4}, \frac{3}{4})$, and 8: $(\frac{3}{4}, \frac{3}{4}, \frac{1}{4})$. Highlighted are the basis vectors of the IR Γ_5, according to which the magnetic ordering is occurring in both studied compounds.

IR	Atom (Co1)	BV $(m_{\|a}, m_{\|b}, m_{\|c})$	Atom (Co2)	BV $(m_{\|a}, m_{\|b}, m_{\|c})$
			5	110
			6	$\bar{1}10$
	1	001	7	$1\bar{1}0$
Γ_3	2	001	8	$\bar{1}\bar{1}0$
	3	001	5	001
	4	001	6	001
			7	001
			8	001
			5	110
			6	$1\bar{1}0$
	1	**001**	7	$\bar{1}10$
Γ_5	**2**	**$00\bar{1}$**	8	$\bar{1}\bar{1}0$
	3	**$00\bar{1}$**	**5**	**001**
	4	**001**	**6**	**$00\bar{1}$**
			7	**$00\bar{1}$**
			8	**001**
			5	100
			6	100
			7	100
			8	100
	1	100	5	010
	2	100	6	$0\bar{1}0$
	3	100	7	$0\bar{1}0$
	4	100	8	010
	1	010	5	00
	2	$0\bar{1}0$	6	$00\bar{1}$
	3	$0\bar{1}0$	7	001
Γ_9	4	010	8	$00\bar{1}$
	1	$0\bar{1}0$	5	$0\bar{1}0$
	2	$0\bar{1}0$	6	$0\bar{1}0$
	3	$0\bar{1}0$	7	$0\bar{1}0$
	4	$0\bar{1}0$	8	$0\bar{1}0$
	1	$\bar{1}00$	5	$\bar{1}00$
	2	100	6	100
	3	100	7	100
	4	$\bar{1}00$	8	$\bar{1}00$
			5	$00\bar{1}$
			6	$00\bar{1}$
			7	001
			8	001

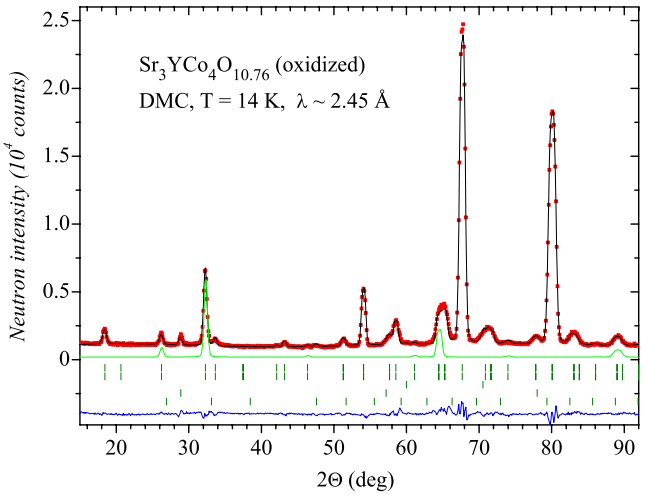

FIG. 8. (Color online) Rietveld refinement of the $T=14$ K DMC data of the $Sr_3YCo_4O_{10.76}$ (Y314-oxidized) compound. The five rows of ticks below the graph correspond to: main Y314 chemical structure, its *G*-type magnetic structure, CoO impurity, its magnetic phase, Y_2O_3 impurity. The solid green line is the contribution of neutron diffraction on the solely magnetic Y314 structure into the total calculated intensity.

Other possibilities which cannot be completely excluded based on solely the powder diffraction data are: the existence of the in-plane components of magnetic moments of the Co2 ions and the presence of the ferromagnetic component in the magnetic ordering scheme of the investigated Y-314 phases, i.e., the admixture of another irreducible representation. These possibilities however, even if considered—would only slightly change the determined magnetic structure—i.e., the main ordering scheme is the one described above, and all the possible "imperfections" thereof may only give rise to the extremely minor, in fact indefinable from the powder diffraction data corrections.

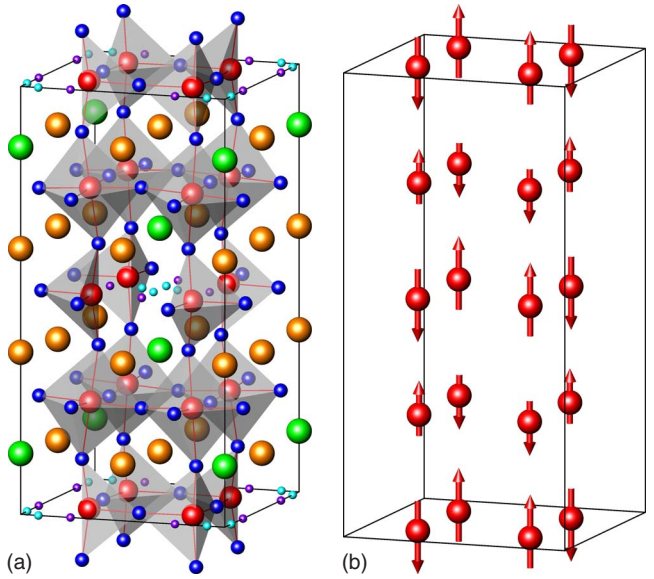

FIG. 9. (Color online) Illustration of the crystal and magnetic structures of the $Sr_3YCo_4O_{10.52}$ and $Sr_3YCo_4O_{10.76}$ (valid for both the as-prepared and oxidized samples). For simplicity, only the tetrahedral coordination is shown for the Co1 ions. In reality, also the incomplete bipyramidal coordination (via the O2 and O2′ atoms shown in the figure with smaller size circles) is equally possible—see the text and Fig. 4 for details. The ratio between the magnetic moment magnitudes in this figure corresponds to the one found in the oxidized compound at $T=14$ K.

Thus, within the accuracy of the experiment and data treatments, the magnetic structure is antiferromagnetic, of the "*G* type" (in notations of the magnetic structures accepted for the three-dimensional perovskite manganese oxides[26]), with magnetic Co moments being aligned along the *c* axis of the unit cell, and with the moment magnitudes located on the Co1 sites (in the layers with $z=0$ and $\frac{1}{2}$, correspondingly) differing by roughly a factor of 2 from those on the Co2 sites in the layers with $z=\frac{1}{4}$ and $\frac{3}{4}$ (see Fig. 9). This scheme generally corresponds to the previously reported one for the 314 phases,[8,11] introducing, however, an important correction concerning the different magnitudes of the magnetic moments on the Co1 and Co2 sites. The temperature dependences of magnetic moments for both sublattices in all the samples are shown in Fig. 10.

We definitely register strongly different magnetic moment magnitudes for the two Co sites with different effective coordination. The AFM transition temperatures derived from the neutron powder diffraction data are: $T_N \sim 342(\pm 7)$ K for the as-prepared $Sr_3YCo_4O_{10.52}$ compound and $T_N \sim 299(\pm 5)$ K for the oxidized $Sr_3YCo_4O_{10.76}$ material. Interestingly enough that such significant lowering of the AFM transition temperature is only caused by tiny oxygen stoichiometry modifications, which are practically not influencing the majority of the crystal structure parameters (Tables II and III). Another observation is that the increase in the oxidation state of cobalt from +3.01 to +3.13 by introducing of oxygen atoms in the O2 and O2′ positions leads to the decrease in the magnetic moments of cobalt in nearly equal amount for both Co1 and Co2 atoms (Fig. 10).

The magnetic structure determination carried out from the neutron powder diffraction data and supported by the macroscopic measurements has shown that both compounds are the G-type antiferromagnets. An important correction to the results published before (Refs. 8 and 11) is that in fact the magnetic moments of the Co ions in the less-oxidized oxygen-deficient layers (on the Co1 sites) are significantly higher than these of the more-oxidized Co ions with the completely filled octahedral coordination (located on the Co2 sites). Thus, in our study, we have experimentally observed ordering of different spin states of Co cations over the positions with the complete octahedral and oxygen-deficient coordinations and hence with presumably different charge states.

IV. SUMMARY

In summary, we have prepared $Sr_3YCo_4O_{10.5+\delta}$ compounds with the so-called "314-phase" structure ($I4/mmm$, $a \approx 2 \times a_{per}$, $c \approx 4 \times a_{per}$) possessing different oxygen content corresponding to $\delta=0.02$ and 0.26, and studied the temperature evolution of their crystal and magnetic structures by

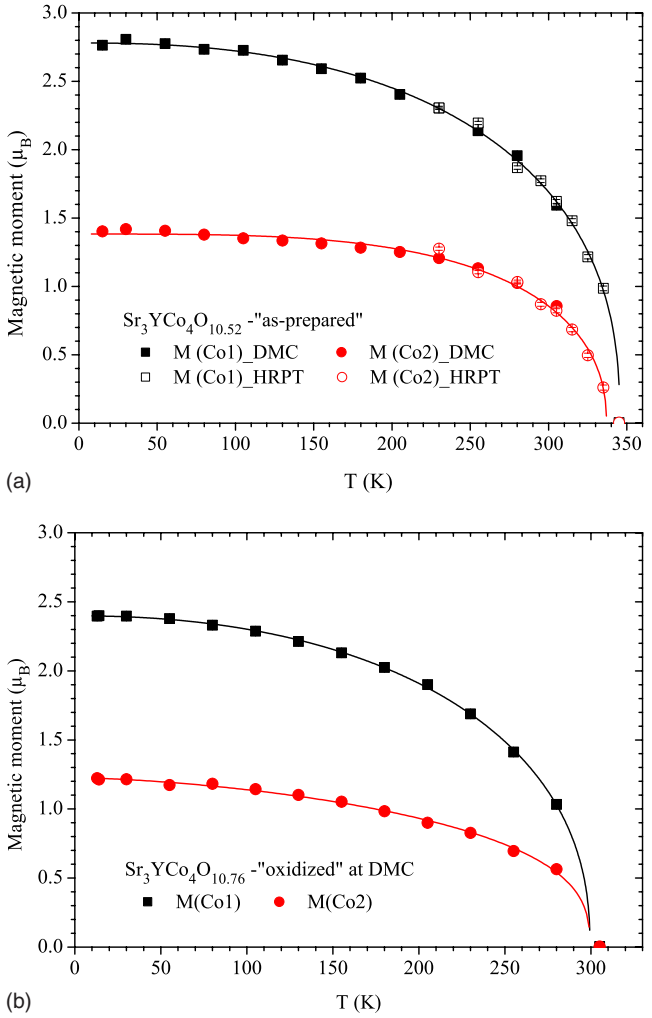

FIG. 10. (Color online) Refined magnetic moments on the Co1 (squares) and Co2 (circles) sites for the investigated compounds: $Sr_3YCo_4O_{10.52}$ (as prepared—panel *a*) and $Sr_3YCo_4O_{10.76}$ (oxidized—panel *b*). The lines are guides to the eye. Filled circles correspond to the results obtained with DMC diffractometer ($\lambda = 2.45$ Å), opened ones—to the results from HRPT diffractometer ($\lambda = 2.955$ Å).

neutron powder diffraction. In contrast to the previous studies, refinement of the crystal structure of the as-prepared ($\delta = 0.02$) 314 phase revealed different distribution of oxygen atoms in the oxygen-deficient layer over both the O2 and O2′ positions (Fig. 4). The main reason for this could be a considerable disorder of Sr^{2+} and Y^{3+} in the crystal structure and the degree of disorder could be associated to the amount of oxygen in the O2′ position. The study of the temperature evolution of the crystal structure of $Sr_3YCo_4O_{10.5+\delta}$, $\delta = 0.02$ and 0.26 revealed an increase in the thermal-expansion anisotropy of the structure ($\alpha_c \gg \alpha_a$) with temperature. We found that the most probable cause for such behavior is the temperature dependence of the apical (directed along the *c* axis of the tetragonal unit cell) Co2-O1 interatomic distance in the completely filled $Co2(O1,O4)_6$ octahedra.

Oxidation of the 314 phase leads to the decrease in the T_N from ~342(±7) K for the as-prepared $Sr_3YCo_4O_{10.52}$ compound to ~299(±5) K for the oxidized $Sr_3YCo_4O_{10.76}$ one. Our study of the magnetic structure confirmed the *G*-type AFM ordering, with the magnetic Co moments being aligned along the *c* axis of the tetragonal cells. In contrast to the previous results we have experimentally observed the ordering of different spin states of Co over the positions in the differently oxidized octahedral and oxygen-deficient Co layers with the magnetic moments of the Co ions in the oxygen-deficient layers being significantly higher than those of the Co ions in the completely filled octahedral coordination. Thus, we demonstrate a direct correlation of the spin and charge orderings in these novel cobaltites.

ACKNOWLEDGMENTS

This work is based on the experiments carried out at the Swiss Spallation Neutron Source SINQ, Paul Scherrer Institut, Villigen, Switzerland. S.Ya.I. would like to acknowledge RFBR (Grant No. 08-03-00919-a) for the financial support.

*denis.sheptyakov@psi.ch

[1] C. Martin, A. Maignan, D. Pelloquin, N. Nguyen, and B. Raveau, Appl. Phys. Lett. **71**, 1421 (1997).
[2] J. B. Goodenough, J. Phys. Chem. Solids **6**, 287 (1958).
[3] P. M. Raccah and J. B. Goodenough, Phys. Rev. **155**, 932 (1967).
[4] M. A. Señarís-Rodríguez and J. B. Goodenough, J. Solid State Chem. **116**, 224 (1995).
[5] P. G. Radaelli and S.-W. Cheong, Phys. Rev. B **66**, 094408 (2002).
[6] S. Y. Istomin, J. Grins, G. Svensson, O. A. Drozhzhin, V. L. Kozhevnikov, E. V. Antipov, and J. P. Attfield, Chem. Mater. **15**, 4012 (2003).
[7] R. L. Withers, M. James, and D. J. Goossens, J. Solid State Chem. **174**, 198 (2003).
[8] S. Y. Istomin, O. A. Drozhzhin, G. Svensson, and E. V. Antipov, Solid State Sci. **6**, 539 (2004).
[9] M. James, D. Cassidy, D. J. Goossens, and R. L. Withers, J. Solid State Chem. **177**, 1886 (2004).
[10] L. J. Gillie, H. M. Palmer, A. J. Wright, J. Hadermann, G. Van Tendeloo, and C. Greaves, J. Phys. Chem. Solids **65**, 87 (2004).
[11] D. J. Goossens, K. F. Wilson, M. James, A. J. Studer, and X. L. Wang, Phys. Rev. B **69**, 134411 (2004).
[12] R. Caciuffo, D. Rinaldi, G. Barucca, J. Mira, J. Rivas, M. A. Señarís-Rodríguez, P. G. Radaelli, D. Fiorani, and J. B. Goodenough, Phys. Rev. B **59**, 1068 (1999).
[13] A. Maignan, S. Hebert, V. Caignaert, V. Pralong, and D. Pelloquin, J. Solid State Chem. **178**, 868 (2005).

[14] W. Kobayashi, S. Ishiwata, I. Terasaki, M. Takano, I. Grigoraviciute, H. Yamauchi, and M. Karppinen, Phys. Rev. B **72**, 104408 (2005).
[15] Y. F. Zhang, S. Sasaki, O. Yanagisawa, and M. Izumi, Acta Phys. Pol. A **111**, 79 (2007).
[16] Y. F. Zhang, S. Sasaki, O. Yanagisawa, and M. Izumia, J. Magn. Magn. Mater. **310**, 1002 (2007).
[17] W. Kobayashi, S. Yoshida, and I. Terasaki, Prog. Solid State Chem. **35**, 355 (2007).
[18] A. Baszczuk, S. Kolesnik, B. Dabrowski, O. Chmaissem, and J. Mais, Phys. Rev. B **76**, 134407 (2007).
[19] P. Fischer *et al.*, Physica B **276-278**, 146 (2000).
[20] P. Fischer, L. Keller, J. Schefer, and J. Kohlbrecher, Neutron News **11**, 19 (2000).
[21] J. Rodríguez-Carvajal, Physica B **192**, 55 (1993).
[22] F. Lindberg, O. A. Drozhzhin, S. Y. Istomin, G. Svensson, F. B. Kaynak, P. Svedlindh, P. Warnicke, A. Wannberg, A. Mellergard, and E. V. Antipov, J. Solid State Chem. **179**, 1434 (2006).
[23] S. Fukushima, T. Sato, D. Akahoshi, and H. Kuwahara, J. Appl. Phys. **103**, 07F705 (2008).
[24] S. Y. Istomin, O. A. Drozhzhin, P. S. Napolsky, S. N. Putilin, A. A. Gippius, and E. V. Antipov, Solid State Ion. **179**, 1054 (2008).
[25] A. Wills, Physica B **276-278**, 680 (2000), program available from www.ccp14.ac.uk
[26] E. O. Wollan and W. C. Koehler, Phys. Rev. **100**, 545 (1955).